G. L. Gray
Assistant Professor,
Department of Engineering Science
and Mechanics,
The Pennsylvania State University,
227 Hammond Building,
University Park, PA 16802-1401
e-mail: gray@engr.psu.edu
Mem. ASME

D. C. Kammer
Associate Professor,
Department of Engineering Physics,
University of Wisconsin-Madison,
1500 Engineering Drive,
Madison, WI 53706-1687
e-mail: kammer@coefac.engr.wisc.edu
Mem. ASME

I. Dobson
Associate Professor,
Department of Electrical and
Computer Engineering,
University of Wisconsin-Madison,
1415 Engineering Drive,
Madison, WI 53706-1691
e-mail: dobson@engr.wisc.edu

A. J. Miller
Graduate Student,
Department of Engineering Science
and Mechanics,
The Pennsylvania State University,
227 Hammond Building,
University Park, PA 16802-1401
e-mail: ajm138@psu.edu

Heteroclinic Bifurcations in Rigid Bodies Containing Internally Moving Parts and a Viscous Damper

Melnikov's method is used to analytically study chaotic dynamics in an attitude transition maneuver of a torque-free rigid body in going from minor axis to major axis spin under the influence of viscous damping and nonautonomous perturbations. The equations of motion are presented, their phase space is discussed, and then they are transformed into a form suitable for the application of Melnikov's method. Melnikov's method yields an analytical criterion for homoclinic chaos in the form of an inequality that gives a necessary condition for chaotic dynamics in terms of the system parameters. The criterion is evaluated for its physical significance and for its application to the design of spacecraft. In addition, the Melnikov criterion is compared with numerical simulations of the system. The dependence of the onset of chaos on quantities such as body shape and magnitude of damping are investigated. In particular, it is found that for certain ranges of viscous damping values, the rate of kinetic energy dissipation goes down when damping is increased. This has a profound effect on the criterion for chaos.

Introduction

The determination and control of attitude evolution are important problems in modern spacecraft dynamics. The equations of motion describing the attitude dynamics of complex nonrigid spacecraft can be derived, but their analytical solution is elusive. Solutions to these highly nonlinear equations can be obtained using numerical simulation, but many interesting features of the dynamics can be lost in the numerical data. Fortunately, a great deal of physical insight into the behavior of these complex systems can be obtained by using a simpler "rigid body with perturbations" approximation for the spacecraft. This paper deals with the dynamics of the attitude transition from minor axis to major axis spin of a viscously damped, rigid body that is being perturbed by small oscillating masses. In particular, chaotic dynamics occurring during spin-axis transition will be investigated. We obtain an analytical test for chaos in terms of system parameters.

A single-body spacecraft is directionally unstable in the presence of energy dissipation when perturbed from spinning about its minor axis (Hughes, 1986). In the absence of active stabilization, the body will eventually reorient itself and spin about the major axis. Oscillating subbodies can produce chaos in a region of the phase space traversed by the spacecraft during this attitude maneuver. It is often important to be able to accurately predict the timing of this attitude maneuver and the presence of chaotic dynamics could render useless any attempt at this prediction. Therefore we suggest the spacecraft be designed such that chaos is avoided. It should be noted that the type of chaos considered herein is transient in nature and is distinct from chaos in a strange attractor (Guckenheimer and Holmes, 1983), though numerical investigations show that it can, in many cases, be difficult to tell the difference between strange attractor-type chaos and the type of chaos exhibited by these spacecraft models (Campbell, 1997).

Some aspects of related attitude maneuvers have been studied for dual-spin spacecraft. These spacecraft are reoriented by spin-up of rotors relative to the main spacecraft body. Attitude resonances in this maneuver, occurring during the spin-up or spin-down, have been investigated using perturbation techniques and numerical simulation (see, for example, Adams, 1980; Barba and Aubrun, 1976; Cochran and Holloway, 1980; Gebman and Mingori, 1976; Hall and Rand, 1994; Or, 1991; Or, 1998b). In addition, Or (1998a) has studied chaotic dynamics in dual-spin spacecraft using Melnikov's method, though Or does little in the way of interpreting these results.

In the case of single-body satellites, the direction and control of the final major axis orientation have been studied (Barba et al., 1973; Chinnery and Hall, 1995; Cronin, 1978; Kaplan and Cenker, 1973; Levi, 1989; Rahn and Barba, 1991), as have the dynamics

Contributed by the Applied Mechanics Division of THE AMERICAN SOCIETY OF MECHANICAL ENGINEERS for publication in the ASME JOURNAL OF APPLIED MECHANICS.
Discussion on the paper should be addressed to the Technical Editor, Professor Lewis T. Wheeler, Department of Mechanical Engineering, University of Houston, Houston, TX 77204-4792, and will be accepted until four months after final publication of the paper itself in the ASME JOURNAL OF APPLIED MECHANICS.
Manuscript received by the ASME Applied Mechanics Division, Oct. 15, 1997; final revision, Feb. 14, 1999. Associate Technical Editor: N. C. Perkins.

and evolution of the maneuver itself, as found in Tsiotras and Longuski (1991) and Longuski and Tsiotras (1993a, b), in which they study the attitude evolution of near-symmetric rigid bodies under a variety of torque conditions. So far, little work has investigated the fundamental nature and causes of the observed and predicted dynamics. The work herein is another step in the process of obtaining that understanding.

The non-Hamiltonian perturbations of the rigid-body dynamics dealt with in this paper are due to time-periodic enforced motions of subbodies and viscous damping within a single rigid-body satellite. While the occurrence of chaos in this class of systems is not surprising (Lichtenberg and Lieberman, 1992), our application of Melnikov's method to detect the onset of chaos in this class of systems is new. As with earlier work (Gray et al., 1992, 1996), we have overcome considerable difficulties in model formulation and in the application of Melnikov's method to obtain a criterion for chaos which can be used in spacecraft design. Some of the closely related work is limited to chaos in spacecraft attitude dynamics when the perturbations are Hamiltonian (Dovbysh, 1989; Holmes and Marsden, 1983; Koiller, 1984). Some work has been done for non-Hamiltonian perturbations to spacecraft dynamics, but it has dealt almost exclusively with the stability of equilibria (Baillieul and Levi, 1987; Krishnaprasad, 1985; Krishnaprasad and Marsden, 1987; Rubanovskii, 1988). In other recent work, Tong and Tabarrok (1997) use Melnikov's method to investigate the the attitude motion of self-excited rigid bodies subject to small perturbation torques in a viscous medium. In contrast, the non-Hamiltonian perturbations studied in the current work are explicit functions of time, resulting in equations of motion with time-dependent coefficients, and in which the damping is implemented via internal viscosity. This class of perturbations is of considerable practical importance in spacecraft design. For example, the enforced time-dependent motion can include reciprocating masses, unbalanced rotors with constant angular velocities, and rotors with time-dependent spin rates.

Melnikov's method has been recently applied by Gray et al. (1992, 1996, 1998) to a problem which is similar to the one considered in this paper. The damping was assumed to be small and was implemented through a quantitative energy sink such that additional degrees-of-freedom would not be added to the system. A criterion was derived in terms of the system's physical parameters for the existence of chaos. This investigation considers a more realistic case consisting of larger damping that is implemented using an actual damping mechanism onboard the rigid body. Considering a physical damping mechanism greatly complicates the analysis. The current work, therefore, extends and complements our earlier investigations and serves as a paradigm for the study of a large class of problems that are "close" to the free rigid body.

Rigid-Body Model

The model used in this study is a torque-free, viscously damped rigid body that is perturbed by time-dependent subbody motion. Viscous damping is implemented by a rotor immersed in a viscous fluid within the rigid body. The subbodies and the angular momentum of the rotor relative to the platform are assumed to have a small, $\mathcal{O}(\epsilon)$ effect on the rigid carrier body and are therefore not included in the dynamics of the unperturbed system. The specific rigid body model is shown in Fig. 1.

The model is described as follows: The system's mass center c does not move relative to the carrier body since the two subbodies oscillate symmetrically with respect to c along the x-axis. The position of the subbodies relative to the carrier is a known periodic function of time and is denoted by $\eta(t)$. The $\eta = 0$ position is located a distance l from the mass center c. We let x, y, z denote a body-fixed orthogonal coordinate system aligned with the principal axes of the carrier body and centered at c. The principal moments of inertia of the carrier and the rotor with respect to c are designated I_1, I_2, I_3. The moments of inertia are distinct and we

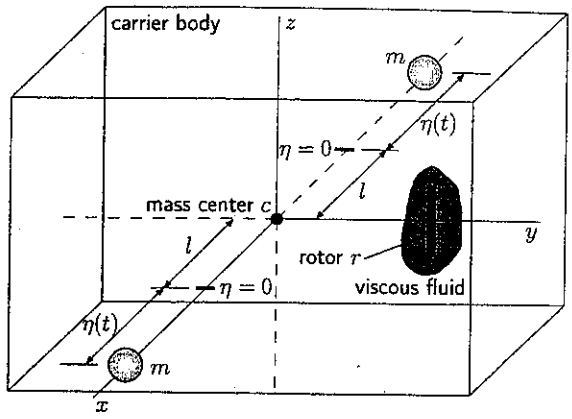

Fig. 1 The model rigid-body configuration

assume $I_1 < I_2 < I_3$. The mass center of the rotor lies on the y-axis and its spin axis is aligned with the y-axis. The rotor is immersed in a cavity containing a viscous fluid with a coefficient of viscous damping γ. The rotor spins relative to the carrier body with angular velocity ω_r and its moment of inertia about the y-axis is I_r.

In order to apply Melnikov's method, it is assumed that the subbodies of mass m are "small" in comparison to the main body. In addition, the angular momentum of the rotor with respect to the carrier body is assumed to be "small." What we mean by "small" will be defined later with respect to a perturbation parameter ϵ. Therefore, both the subbodies and the rotor angular momentum are assumed to have an $\mathcal{O}(\epsilon)$ perturbing effect on the rigid carrier body.

Equations of Motion

Using standard methods such as Lagrange's equations or Newton-Euler techniques, and defining the following principal body angular momentum components h_1, h_2, h_3,

$$h_1 = A\omega_1 \quad h_2 = B\omega_2 + I_r\omega_r \quad h_3 = C\omega_3,$$

the equations of motion can be written as

$$\dot{h}_1 = \frac{1}{B+\Delta}\left(I_r\omega_r h_3 - \frac{C-B}{C+\Delta}h_2h_3\right) \tag{1}$$

$$\dot{h}_2 = \left(\frac{1}{A} - \frac{1}{C+\Delta}\right)h_1h_3 \tag{2}$$

$$\dot{h}_3 = \left(\frac{1}{B+\Delta} - \frac{1}{A}\right)h_1h_2 - \frac{I_r}{B+\Delta}\omega_r h_1 \tag{3}$$

$$\dot{\omega}_r = \frac{1}{I_r - B - \Delta}\left[\left(\frac{1}{A} - \frac{1}{C+\Delta}\right)h_1h_3 + \frac{\gamma}{I_r}(B+\Delta)\omega_r - \dot{\Delta}\left(\frac{h_2 - I_r\omega_r}{B+\Delta}\right)\right] \tag{4}$$

where $A \triangleq I_1$, $B \triangleq I_2 + 2ml^2$, $C \triangleq I_3 + 2ml^2$, $\Delta = \Delta(t) \triangleq 2m\eta(t)[2l + \eta(t)]$, and $\dot{(\,)}$ denotes differentiation with respect to time. Note that Δ is the term that embodies the assumed to be known, time-dependent subbody motion (i.e., known frequency and amplitude).

It is now convenient to nondimensionalize the equations of motion and explicitly introduce the perturbation parameter ϵ. This makes clearer which terms are small, and therefore higher order, and which terms are to be retained. Defining the following nondimensional quantities

$$\epsilon \triangleq ml^2/B \qquad \tau \triangleq Ht/B \quad \tilde{h}_i \triangleq h_i/H \quad \tilde{h}_i' \triangleq \left(\frac{B}{H^2}\right)\dot{h}_i$$

$$\tilde{\Delta} \triangleq \frac{\Delta}{\epsilon B} \qquad \bar{\gamma} \triangleq \gamma/H \quad r_1 \triangleq C/B \quad r_2 \triangleq A/B$$

$$\tilde{\omega}_r \triangleq \left(\frac{B}{H\sqrt{\epsilon}}\right)\omega_r \quad \bar{I}_r \triangleq \frac{I_r}{B\sqrt{\epsilon}} \quad \tilde{h}_r \triangleq \bar{I}_r\tilde{\omega}_r \quad \tilde{\omega}_r' \triangleq \left(\frac{B^2}{H^2\sqrt{\epsilon}}\right)\dot{\omega}_r,$$

where H is the magnitude of the angular momentum vector, the equations of motion, Eqs. (1)–(4), become

$$\tilde{h}_1' = \frac{1}{1+\epsilon\tilde{\Delta}}\left(\epsilon\tilde{h}_r\tilde{h}_3 - \frac{r_1-1}{r_1+\epsilon\tilde{\Delta}}\tilde{h}_2\tilde{h}_3\right) \tag{5}$$

$$\tilde{h}_2' = \left(\frac{1}{r_2} - \frac{1}{r_1+\epsilon\tilde{\Delta}}\right)\tilde{h}_1\tilde{h}_3 \tag{6}$$

$$\tilde{h}_3' = \left(\frac{1}{1+\epsilon\tilde{\Delta}} - \frac{1}{r_2}\right)\tilde{h}_1\tilde{h}_2 - \frac{\epsilon}{1+\epsilon\tilde{\Delta}}\tilde{h}_r\tilde{h}_1 \tag{7}$$

$$\tilde{\omega}_r' = \frac{-\left[\left(\frac{1}{r_2} - \frac{1}{r_1+\epsilon\tilde{\Delta}}\right)\tilde{h}_1\tilde{h}_3 + \bar{\gamma}(1+\epsilon\tilde{\Delta})\frac{\tilde{\omega}_r}{\bar{I}_r} - \epsilon\tilde{\Delta}'\left(\frac{\tilde{h}_2-\epsilon\tilde{h}_r}{1+\epsilon\tilde{\Delta}}\right)\right]}{\sqrt{\epsilon}-\epsilon\bar{I}_r+\epsilon^{3/2}\tilde{\Delta}} \tag{8}$$

Equations (5)–(8) are the full equations of motion with no simplifying assumptions. As will be seen, these equations must be transformed into a form consisting of an unperturbed part[1] plus perturbation terms in order to apply Melnikov's method. This is done by expanding the equations in powers of ϵ and keeping terms through $\mathcal{O}(\epsilon)$. The expanded equations can be written as

$$\tilde{h}_1' = \frac{1-r_1}{r_1}\tilde{h}_2\tilde{h}_3 + \epsilon\left[\tilde{h}_r\tilde{h}_3 + \tilde{\Delta}\left(\frac{r_1^2-1}{r_1^2}\right)\tilde{h}_2\tilde{h}_3\right] + O(\epsilon^2) \tag{9}$$

$$\tilde{h}_2' = \left(\frac{r_1-r_2}{r_1r_2}\right)\tilde{h}_1\tilde{h}_3 + \epsilon\frac{\tilde{\Delta}}{r_1^2}\tilde{h}_1\tilde{h}_3 + O(\epsilon^2) \tag{10}$$

$$\tilde{h}_3' = \left(\frac{r_2-1}{r_2}\right)\tilde{h}_1\tilde{h}_2 - \epsilon(\tilde{\Delta}\tilde{h}_1\tilde{h}_2 + \tilde{h}_r\tilde{h}_1) + O(\epsilon^2) \tag{11}$$

$$\sqrt{\epsilon}\,\tilde{\omega}_r' = -\left(\frac{r_1-r_2}{r_1r_2}\right)\tilde{h}_1\tilde{h}_3 - \bar{\gamma}\frac{\tilde{\omega}_r}{\bar{I}_r} - \sqrt{\epsilon}\left[\left(\frac{r_1-r_2}{r_1r_2}\right)\bar{I}_r\tilde{h}_1\tilde{h}_3 + \bar{\gamma}\tilde{\omega}_r\right] - \epsilon\left[\left(\frac{r_2-r_1}{r_1r_2}+\frac{1}{r_1^2}\right)\tilde{\Delta}\tilde{h}_1\tilde{h}_3 - \tilde{h}_2\tilde{\Delta}' - \left(\frac{r_2-r_1}{r_1r_2}\right)\bar{I}_r^2\tilde{h}_1\tilde{h}_3 + \bar{\gamma}\bar{I}_r\tilde{\omega}_r\right] + O(\epsilon^{3/2}). \tag{12}$$

The assumed order of various physical quantities gives the form of the equations of motion given above—different assumptions would change the form. In particular, our choice of assumed orders leads to equations of motion for which the unperturbed solution can be obtained. It should be noted that making the assumptions that I_r and ω_r are $\mathcal{O}(\sqrt{\epsilon})$ quantities in no way invalidates our results; it merely reduces the size that we must assign to ϵ when saying that our results are valid "for sufficiently small ϵ."

The Unperturbed Phase Space

In order to apply Melnikov's method to the system of Eqs. (9)–(12), there must be a heteroclinic cycle (Guckenhiemer and Holmes, 1983) in the unperturbed phase space, and the unperturbed system must be integrable. It can be shown that the attitude dynamics of a torque-free rigid body, when measured in body angular momentum components, occur on the surface of the angular momentum sphere (see Fig. 2). This sphere is also the reduced phase space corresponding to Euler's equations of motion for a torque-free rigid body. In terms of the nondimensional quantities defined herein, these equations are given by

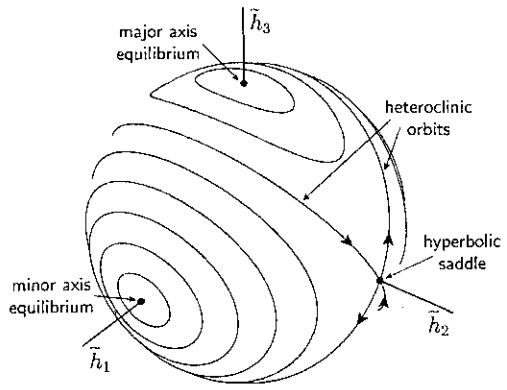

Fig. 2 The momentum sphere illustrating the heteroclinic orbits and the hyperbolic saddle points. The curves are orbits of constant energy.

$$\tilde{h}_1' = \left(\frac{1-r_1}{r_1}\right)\tilde{h}_2\tilde{h}_3 \tag{13}$$

$$\tilde{h}_2' = \left(\frac{r_1-r_2}{r_1r_2}\right)\tilde{h}_1\tilde{h}_3 \tag{14}$$

$$\tilde{h}_3' = \left(\frac{r_2-1}{r_2}\right)\tilde{h}_1\tilde{h}_2. \tag{15}$$

Equations (13)–(15) are just the first three equations of motion for the system considered here, Eqs. (5)–(7), with $\epsilon = 0$, i.e., they are the unperturbed equations of motion. Euler's equations are integrable in terms of Jacobi elliptic functions for nearly all admissible values of angular momentum and kinetic energy, but for a given angular momentum, there is a value of kinetic energy such that they are integrable in terms of hyperbolic functions. These integral curves will play a very important role in the following development.

The phase space for Euler's equations is $\mathbb{R}^3$, but the motion is confined to the surface of the momentum sphere. This phase space possesses six fixed points or equilibria corresponding to positive and negative spin about each of the three principal moment of inertia axes of the rigid body. Two of the equilibria correspond to spin about the major principal axes and two correspond to spin about the minor principal axes. Topologically, all four of these equilibria are centers, in that the linearization of Euler's equations at these points has two complex eigenvalues with zero real parts (ignoring the unimportant dimension orthogonal to the surface of the momentum sphere). The other two equilibria correspond to spin about the intermediate principal axes and are hyperbolic fixed points or saddles (the linearization has two real eigenvalues, one positive and one negative). The phase space also has four heteroclinic orbits linking the hyperbolic fixed points, thus giving heteroclinic cycles, as shown in Fig. 2. These heteroclinic orbits are the integral curves that can be written in terms of hyperbolic functions that were described above. During the transition of an energy dissipating rigid body from spin near the minimum moment of inertia axis to spin about the maximum moment of inertia axis, the trajectory must cross the heteroclinic orbits in the phase space. More precisely, the trajectory of the damped system must cross a heteroclinic orbit of the undamped system (the heteroclinic orbits break up in the presence of damping). We study the chaotic motion in the perturbed system that may occur near these heteroclinic orbits.

[1] Found by setting $\epsilon = 0$. The unperturbed equations are just the equations for a torque-free rigid body.

Melnikov's Method and Equation Transformation

Melnikov's method (Melnikov, 1963) is applied to detect chaos in the system of Eqs. (9)–(12). For a detailed exposition of Melnikov theory, see Holmes (1980), Holmes (1981), Guckenheimer and Holmes (1983) or Wiggins (1990). Briefly, Melnikov's method is a perturbation technique for proving the existence of transverse heteroclinic[2] orbits to hyperbolic periodic orbits in a class of time-periodic vector fields. Although it is a perturbation technique, Melnikov's method gives *global* information about the system's dynamics. The existence of transverse heteroclinic orbits implies the existence of horseshoes and chaos via the Smale-Birkhoff theorem. In phase space, the chaos appears near the unperturbed heteroclinic orbit. The essential idea is to use the globally computable solutions to the unperturbed *integrable* system in studying the perturbed solution.

The form of Melnikov's method we are using considers systems of the form

$$\dot{x} = f(x) + \epsilon g(x, t; \mu), \tag{16}$$

where $x \in \mathbb{R}^2$, f is a vector field possessing two hyperbolic fixed points, p_1 and p_2, connected to one another by a heteroclinic orbit, $q_0(t)$ (i.e., $\lim_{t\to\infty} q_0(t) = p_1$ and $\lim_{t\to-\infty} q_0(t) = p_2$), g is a small perturbation of period T in t, and $\mu \in \mathbb{R}^k$ is a vector of parameters. If the Melnikov function is denoted $\mathcal{M}(t_0)$, it can be written as the integral

$$\mathcal{M}(t_0) = \int_{-\infty}^{\infty} \left\{ [f(q_0(t)) \wedge g(q_0(t), t + t_0)] \times \exp\left[-\int_0^t \text{trace}(Df)(q_0(s))ds \right] \right\} dt, \tag{17}$$

where the symbol $\wedge$ is the wedge operator, defined by $a \wedge b = a_1b_2 - a_2b_1$, and $Df = [\partial f_i/\partial x_j]$ is the Jacobian matrix of the first partial derivatives of f. We note that this is not the same Melnikov integral seen in most expositions of the theory as our unperturbed vector field in transformed coordinates is not Hamiltonian.

The unperturbed phase space (the momentum sphere) has the structure necessary (heteroclinic orbits connecting hyperbolic saddles) to apply Melnikov's method. The initial tasks are:

1 solving for the heteroclinic orbit $q_0(t)$ of the unperturbed system (i.e., finding the hyperbolic solutions along the heteroclinic orbits on the surface of the momentum sphere),
2 writing the perturbed equations of motion, Eqs. (9)–(12), in the form of Eq. (16) such that only terms through $\mathcal{O}(\epsilon)$ are kept, and
3 obtaining two independent equations of motion (in convenient coordinates) describing the dynamics on the surface of the momentum sphere.

Unperturbed Heteroclinic Orbits $q_0(t)$. For a torque-free rigid body with equations of motion given by Eqs. (13)–(15), there are two integrals of the motion: momentum and energy. In nondimensional coordinates, these integrals are given by

$$\tilde{h}_1^2 + \tilde{h}_2^2 + \tilde{h}_3^2 = 1 \quad \text{(momentum)} \tag{18}$$

$$\frac{\tilde{h}_1^2}{r_2} + \tilde{h}_2^2 + \frac{\tilde{h}_3^2}{r_1} = \tilde{T} \quad \text{(energy)} \tag{19}$$

where $\tilde{T} \triangleq 2BT/H^2$ is the nondimensional total energy and T is the total energy. Any trajectory on the momentum sphere is determined by the intersection of the momentum sphere S defined by Eq. (18) and the energy ellipsoid $\mathcal{E}$ defined by Eq. (19). Recall that when viewed in body coordinates, the angular momentum vector appears to move such that its tip always remains on a particular intersection of S and $\mathcal{E}$. The radius of S, which is $\bar{H} = 1$, must lie between the smallest and largest semiaxes of the ellipsoid. Since $A < B < C$, or nondimensionally $0 < r_2 < 1 < r_1$,[3] the condition on the radius of S is given by $r_2\tilde{T} < 1 < r_1\tilde{T}$. Since the heteroclinic orbits are formed when the S and $\mathcal{E}$ surfaces are tangent at the points $(0, \pm 1, 0)$, the energy level for the heteroclinic orbits must be given by $T = H^2/(2B)$, or $\tilde{T} = 1$ nondimensionally. The energy integral then becomes

$$\frac{\tilde{h}_1^2}{r_2} + \tilde{h}_2^2 + \frac{\tilde{h}_3^2}{r_1} = 1. \tag{20}$$

Using Eqs. (13)–(15), (18), and (20), it can be shown that the solutions for the $\tilde{h}_i$ along the heteroclinic orbits are given by (also see Hughes, 1986)

$$\tilde{h}_{1u} = s_1 \left[\frac{r_2(1 - r_1)}{r_2 - r_1} \right]^{1/2} \text{sech} \left\{ \left[\frac{(r_2 - 1)(1 - r_1)}{r_1 r_2} \right]^{1/2} \tau \right\} \tag{21}$$

$$\tilde{h}_{2u} = s_2 \tanh \left\{ \left[\frac{(r_2 - 1)(1 - r_1)}{r_1 r_2} \right]^{1/2} \tau \right\} \tag{22}$$

$$\tilde{h}_{3u} = s_3 \left[\frac{r_1(r_2 - 1)}{r_2 - r_1} \right]^{1/2} \text{sech} \left\{ \left[\frac{(r_2 - 1)(1 - r_1)}{r_1 r_2} \right]^{1/2} \tau \right\}, \tag{23}$$

where the subscript u signifies an unperturbed quantity, $\tau = 0$ has been chosen to eliminate constants of integration, and s_1, s_2, s_3 are each ± 1 and are chosen such that their product $s_1s_2s_3 = +1$.

In addition to the unperturbed solutions for the $\tilde{h}_i$, the equation for the rotor must be incorporated. This is done using a technique similar to that used by Holmes (1983) and by Volosov (1962). We were able to integrate Eqs. (9)–(11) to obtain Eqs. (21)–(23) since they decouple from the rotor equation, Eq. (12), when $\epsilon = 0$. Due to this uncoupling, the unperturbed solution for the rotor is readily obtained by using the solutions given in Eqs. (21)–(23). For $\epsilon = 0$, Eq. (12) becomes

$$\left(\frac{r_1 - r_2}{r_1 r_2} \right) \tilde{h}_{1u}\tilde{h}_{3u} + \tilde{\gamma} \frac{\tilde{\omega}_{ru}}{\tilde{I}_r} = 0,$$

and it can be readily seen that

$$\tilde{h}_{ru} = \tilde{I}_r\tilde{\omega}_{ru} = \frac{\tilde{I}_r^2}{\tilde{\gamma}} \left(\frac{r_2 - r_1}{r_1 r_2} \right) \tilde{h}_{1u}\tilde{h}_{3u}. \tag{24}$$

Equation (24) can now be substituted into the perturbations in Eqs. (9)–(11) to obtain the equations to which Melnikov's method is applied. This process of "eliminating" the degree-of-freedom associated with the rotor was facilitated by the assumptions made on the sizes of all the variables and parameters in the system. We are saying that the rotor is a higher-order perturbation to the system dynamics and that Eq. (24) gives the rotor the motion that would occur if the carrier body were *forced* to move as a free rigid body.

Transforming the $\mathcal{O}(\epsilon)$ Equations of Motion. We now transform to spherical coordinates so that the surface of the momentum sphere is mapped to a plane. This is done since Eqs. (9)–(11) are not independent, that is, the *three* equations are describing motion in $\mathbb{R}^2$. Transforming to spherical coordinates will give two independent equations, though the unperturbed part will no longer be Hamiltonian. It is convenient to choose the coordinate transformation so that one of the new coordinates is zero along an unperturbed trajectory. This can easily be done since the heteroclinic orbits are great circles on the momentum sphere.

Consider the heteroclinic orbit that lies in the region $\tilde{h}_1 > 0$ and $\tilde{h}_3 > 0$. The angle ν between the $\tilde{h}_1$–$\tilde{h}_2$ plane and this heteroclinic orbit can be shown to be

[2] The method applies equally well to systems with homoclinic orbits.

[3] The complete condition on r_1 and r_2 is $0 < r_2 < 1 < r_1 < 1 + r_2$.

$$\nu = \arctan\left[\frac{r_1(r_2-1)}{r_2(1-r_1)}\right]^{1/2}. \tag{25}$$

Starting with a set of coordinates ξ_1, ξ_2, ξ_3 aligned with the $\bar{h}_1, \bar{h}_2, \bar{h}_3$ system, rotate the ξ coordinate system through the angle $-\nu$ about the $\bar{h}_2$-axis so that the positive ξ_1-axis pierces the heteroclinic orbit in the region $\bar{h}_1 > 0$, $\bar{h}_3 > 0$. We can then transform from the ξ coordinates to the dimensionless spherical coordinates ϕ and θ to obtain the following equations relating the $\bar{h}_i$, and ν, θ, and ϕ:

$$\bar{h}_1 = \cos\nu\cos\theta\cos\phi - \sin\nu\sin\phi, \tag{26}$$

$$\bar{h}_2 = \sin\theta\cos\phi, \tag{27}$$

$$\bar{h}_3 = \sin\nu\cos\theta\cos\phi + \cos\nu\sin\phi. \tag{28}$$

The θ coordinate is measured in the ξ_1–ξ_2 plane as a positive rotation about the ξ_3-axis and the ϕ coordinate is measured in the "new" ξ_1–ξ_3 plane as a positive rotation about the "new" ξ_1-axis. Also note that there is no radial dependence since the angular momentum sphere has a constant radius. The derivatives with respect to τ are also needed and they are given by

$$\bar{h}_1' = \phi'(-\cos\nu\sin\phi\cos\theta - \sin\nu\cos\phi) - \theta'\cos\nu\sin\theta\cos\phi, \tag{29}$$

$$\bar{h}_2' = \theta'\cos\theta\cos\phi - \phi'\sin\theta\sin\phi, \tag{30}$$

$$\bar{h}_3' = \phi'(\cos\nu\cos\phi - \sin\nu\cos\theta\sin\phi) - \theta'\sin\nu\sin\theta\cos\phi. \tag{31}$$

Equations (26)–(31) are now substituted into Eqs. (9)–(11) and *any* two of the resulting three equations are then solved for θ' and ϕ'. This gives the final two first-order differential equations to which Melnikov's method is applied:

$$\begin{aligned}\theta' = {} & \{(r_1-r_2)\cos\theta\cos\nu\cos 2\phi\sec\phi\sin\nu \\ & + (2r_1r_2 - r_1 - r_2)\sin\phi\}/(r_1r_2) \\ & + \epsilon\{4r_2\tilde{\gamma}\tilde{\Delta}[\cos\theta\cos 2\phi\sec\phi\sin 2\nu + 2\cos^2\nu\sin\phi \\ & - 2\cos^2\theta\sin^2\nu\sin\phi - 2r_1^2\sin^2\theta\sin\phi] \\ & + \tilde{I}_r^2 r_1(r_1-r_2)\sin\theta\tan\phi[\sin 2\nu(-1+\cos 2\theta \\ & + 3\cos 2\phi + \cos 2\theta\cos 2\phi) \\ & + 4\cos\theta\cos 2\nu\sin 2\phi]\}/(8\tilde{\gamma}r_1^2r_2)\end{aligned} \tag{32}$$

$$\begin{aligned}\phi' = {} & \{(r_1-r_2)\cos\nu\sin\nu\sin\theta\sin\phi\}/(r_1r_2) \\ & + \epsilon\{r_2\tilde{\gamma}\tilde{\Delta}\sin\theta[\sin\nu(\cos\theta\cos\phi\sin\nu + \cos\nu\sin\phi) \\ & - r_1^2\cos\theta\cos\phi] + \tfrac{1}{8}r_1(r_1-r_2)\tilde{I}_r^2\cos\theta[\sin 2\nu(-1 \\ & + \cos 2\theta + 3\cos 2\phi + \cos 2\theta\cos 2\phi) \\ & + 4\cos\theta\cos 2\nu\sin 2\phi]\}/(\tilde{\gamma}r_1^2r_2).\end{aligned} \tag{33}$$

These equations are in the form of Eq. (16), or $\phi' = f_1 + \epsilon g_1$ and $\theta' = f_2 + \epsilon g_2$.

Finally, the unperturbed solutions given by Eqs. (21)–(23) must be transformed to this same set of spherical coordinates. This transformation gives

$$\sin\theta_u = \tanh\left\{\left[\frac{(r_2-1)(1-r_1)}{r_1r_2}\right]^{1/2}\tau\right\} \tag{34}$$

$$\cos\theta_u = \operatorname{sech}\left\{\left[\frac{(r_2-1)(1-r_1)}{r_1r_2}\right]^{1/2}\tau\right\} \tag{35}$$

$$\phi_u = 0 \tag{36}$$

along the selected unperturbed heteroclinic orbit.

The Melnikov Function

We begin by prescribing the time-dependent, periodic form of η, by letting $\tilde{\eta} \triangleq \eta/l$, $\tilde{\Omega} \triangleq \Omega B/H$, and $\eta \triangleq \eta_0\cos(\Omega t)$. This definition corresponds to a simple harmonic oscillation of the masses. It follows that the nondimensional form of Δ is

$$\tilde{\Delta} = \tilde{\eta}^2 + 4\tilde{\eta}\cos(\tilde{\Omega}\tau) + \tilde{\eta}^2\cos(2\tilde{\Omega}\tau). \tag{37}$$

Substituting the unperturbed solutions $q_0(\tau)$, specified by Eqs. (34)–(36), into $f(q_0(\tau))$ and $g(q_0(\tau), \tau + \tau_0)$ of Eqs. (32) and (33), carrying out the wedge product, substituting the result into the Melnikov integral given by Eq. (17), noting that the term in the exponential

$$\operatorname{trace}(Df) = \frac{\sin\theta\sin\phi}{r_1r_2}(r_1-r_2)\sin\nu\cos\nu\tan\phi, \tag{38}$$

is zero when evaluated along the unperturbed heteroclinic trajectory (i.e., $\operatorname{trace}(Df)(q_0(s)) = 0$ when $\phi_u = 0$), and finally eliminating terms that are zero due to having an odd integrand, we obtain

$$\begin{aligned}\mathcal{M}(\tau_0) = {} & \frac{C_1^2\tilde{I}_r^2}{\tilde{\gamma}}\int_{-\infty}^{\infty}\operatorname{sech}^4(C_1\tau)d\tau \\ & - 4\tilde{\eta}C_2\sin(\tilde{\Omega}\tau_0)\int_{-\infty}^{\infty}\sin(\tilde{\Omega}\tau)\tanh(C_1\tau)\operatorname{sech}^2(C_1\tau)d\tau \\ & - \tilde{\eta}^2C_2\sin(2\tilde{\Omega}\tau_0)\int_{-\infty}^{\infty}\sin(2\tilde{\Omega}\tau)\tanh(C_1\tau)\operatorname{sech}^2(C_1\tau)d\tau\end{aligned} \tag{39}$$

where

$$C_1 \triangleq \left[\frac{(r_1-1)(1-r_2)}{r_1r_2}\right]^{1/2} \tag{40}$$

$$C_2 \triangleq \left(\frac{r_1-1}{r_1}\right)^2\left(\frac{r_2-r_1-1}{r_1-r_2}\right)\left[\frac{r_1(1-r_2)}{r_2(r_1-1)}\right]^{1/2}. \tag{41}$$

Interestingly, even though the divergence of the transformed unperturbed vector field (given by Eqs. (32) and (33) with $\epsilon = 0$) is *not* equal to zero as it would be for a Hamiltonian system, it *is* zero when it is evaluated along the heteroclinic trajectory. This will be true for Melnikov's method applied to all systems perturbed off of Euler's equations, Eqs. (13)–(15), and then transformed using spherical coordinates (as we have done in Gray et al., 1992, 1996, 1998). That is, one can apply Melnikov's method to the system transformed using spherical coordinates as if the unperturbed system were Hamiltonian.

The evaluation of these integrals can be accomplished via residue theory. Upon carrying out the integration, the following Melnikov function is obtained:

$$\mathcal{M}(\tau_0) = \frac{4\tilde{I}_r^2C_1^4}{3\tilde{\gamma}} - 2\pi\tilde{\Omega}^2\tilde{\eta}C_2\left[\frac{\sin(\tilde{\Omega}\tau_0)}{\sinh[\pi\tilde{\Omega}/(2C_1)]} + \tilde{\eta}\frac{\sin(2\tilde{\Omega}\tau_0)}{\sinh(\pi\tilde{\Omega}/C_1)}\right]. \tag{42}$$

Melnikov theory states that the condition for transverse heteroclinic orbits and therefore chaos is that $\mathcal{M}(\tau_0)$ change sign for some τ_0 (Guckenheimer and Holmes, 1983). Inspection of the Melnikov function reveals that there are two harmonic terms, one

with twice the frequency of the other. Therefore, the maximum amplitude of the factor containing the harmonic terms is some function F_{max} of *both* of the harmonic amplitudes. It can be shown that F_{max} is given by

$$F_{max} = \frac{1}{4}\left[3A + \sqrt{A^2 + 32B^2}\right] \times \left[\frac{1}{2} + \frac{A}{32B^2}\left(\sqrt{A^2 + 32B^2} - A\right)\right]^{1/2} \quad (43)$$

where $A = \text{csch}\,[\pi\tilde{\Omega}/(2C_1)]$ and $B = \tilde{\eta}\ \text{csch}\ (\pi\tilde{\Omega}/C_1)$. The analytical criterion for chaos becomes

$$2\pi\tilde{\Omega}^2\tilde{\eta}|C_2 F_{max}| > \frac{4\tilde{I}_r^2 C_1^4}{3\tilde{\gamma}}. \quad (44)$$

Close inspection of Eq. (44) reveals that since $C_1 = C_1(r_1, r_2)$, $C_2 = C_2(r_1, r_2)$, and $F_{max} = F_{max}(r_1, r_2, \tilde{\eta}, \tilde{\Omega})$, Eq. (44) is a function of the six system parameters, r_1, r_2, $\tilde{I}_r$, $\tilde{\eta}$, $\tilde{\Omega}$, and $\tilde{\gamma}$. If Eq. (44) is satisfied, then the system modeled by Eqs. (5)–(8) exhibits chaotic dynamics near the heteroclinic orbits for sufficiently small ϵ.

Numerical Simulations

A complete numerical investigation of this system is far beyond the scope of this paper and will be presented in future work. On the other hand, we include some of numerical simulations to attempt to demonstrate the range of validity of Melnikov's method on a system such as the one considered herein. A representative example of the result of some of our numerical simulations is shown in Fig. 3. This figure shows how variations in the nondimensional forcing frequency $\tilde{\Omega}$ (vertical axis in each part) versus the nondimensional damping coefficient forcing amplitude $\tilde{\gamma}$ (horizontal axis in each part) affect the rigid-body motion. In addition, the nondimensional forcing amplitude is given by $\tilde{\eta} = 0.100$ in the top figure, $\tilde{\eta} = 0.575$ in the middle figure, and $\tilde{\eta} = 1.25$ (Yes, the masses do pass through one another.) in the bottom figure. The other system parameters have been fixed at $r_1 = 1.5$, $r_2 = 0.6$, and $\tilde{I}_r = 1.0$. In each part of this figure, the solid black dots indicate trajectories which are chaotic, the open circles indicate limit cycle trajectories (of various periods), and the "pluses" indicate trajectories which damp to major axis spin. Superimposed on the this figure is a black line indicating the boundary between regions of phase space predicted to be chaotic according to Melnikov's method and those that are not. Points to the right of the Melnikov curve are those predicted to be chaotic according to Eq. (44) for this set of system parameters.

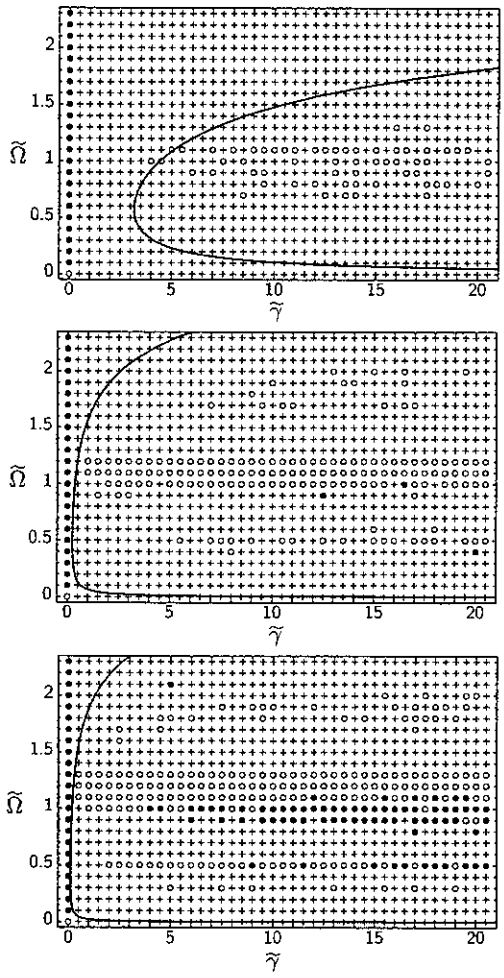

Fig. 3 Three frames in a parameter space evolution showing nondimensional frequency $\tilde{\Omega}$ versus nondimensional viscous damping. From top to bottom, the three plots show $\tilde{\eta} = 0.100$, $\tilde{\eta} = 0.575$, $\tilde{\eta} = 1.25$. See text for further details.

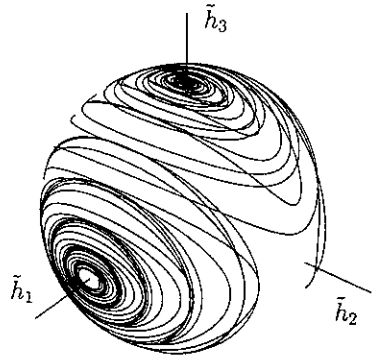

Fig. 4 Major axis spin trajectory where $\tilde{\gamma} = 5.0$, $\tilde{\Omega} = 0.10$, $\tilde{\eta} = 0.9$, $r_1 = 1.5$, $r_2 = 0.6$, and $\tilde{I}_r = 1.0$

To generate this figure, many phase space trajectories were generated and visually examined. This visual examination clearly showed three different classes of trajectories: those that simply decayed to major axis spin (Fig. 4), those that settled into some type of limit cycle (Fig. 5), and those that were chaotic (Fig. 6). It is, of course, impractical to follow this procedure for the approximately 60,000 different parameters sets we have investigated. Consequently, we have devised a "physically intuitive" scheme for automatically selecting between the three types of motion for each trajectory. We utilize the ordinary differential equation solver, lsode (Hindmarsh, 1983), integrate for 2^{16} nondimensional time intervals, and include three statistical measures in the code. These three statistical measures are as follows:

Measure I. When a rigid body reorients itself from minor axis to major axis spin, the angular momentum component in the $\tilde{h}_1$ and

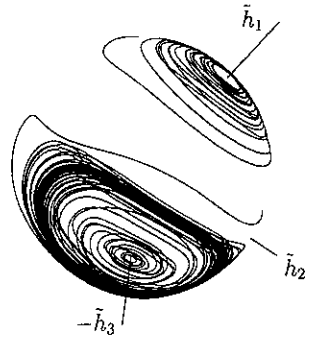

Fig. 5 Periodic trajectory where $\tilde{\gamma} = 5.0$, $\tilde{\Omega} = 1.1$, $\tilde{\eta} = 0.9$, $r_1 = 1.5$, $r_2 = 0.6$, and $\tilde{I}_r = 1.0$

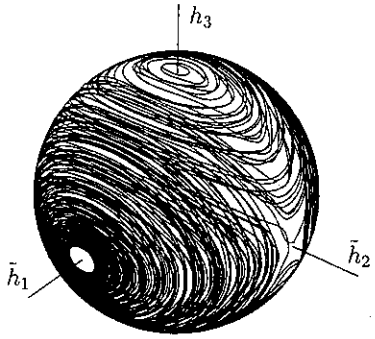

Fig. 6 Chaotic trajectory where $\tilde{\gamma} = 25.0$, $\tilde{\Omega} = 1.0$, $\tilde{\eta} = 0.9$, $r_1 = 1.5$, $r_2 = 0.6$, and $\tilde{I}_r = 1.0$

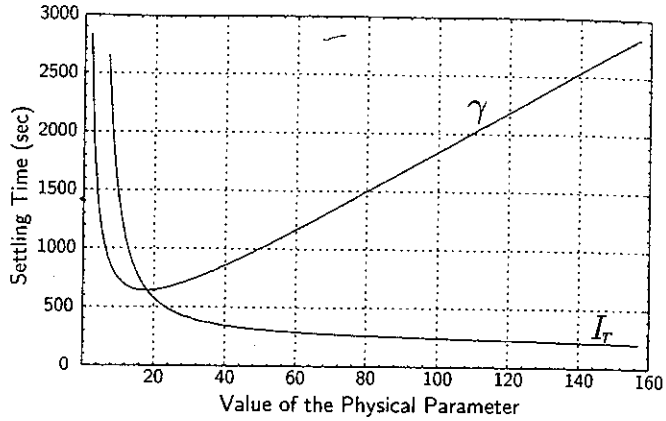

Fig. 7 Time required for the kinetic energy to decay through 95 percent of the difference between the initial kinetic energy and the minimum kinetic energy state. For the γ curve, $I_r = 18.0$ and for the I_r curve, $\gamma = 20.0$.

$\tilde{h}_2$-direction should be very nearly zero and in the $\tilde{h}_3$-direction should be close to one. However, chaotic trajectories often spin about the major axis for a sizable period of time before they depart to another portion of the momentum sphere. Therefore, we need to know if the angular momentum components $\tilde{h}_1$ and $\tilde{h}_2$ have a small variance for a substantial period of time near the end of the integration time period. The exact condition we used is that the variances $\sigma^2(\tilde{h}_1)$ and $\sigma^2(\tilde{h}_2)$ are both less than 0.001 for the last two percent of the integration time.

Measure II. When the satellite's trajectory degenerates into a limit cycle on the surface of the momentum sphere, the path is not a circle in $\mathbb{R}^2$, but a curve in $\mathbb{R}^3$. In this case periodic orbits are bounded by the unperturbed heteroclinic orbits and follow the curvature of the momentum sphere. Consequently a limit cycle ends up being periodic in all three of its angular momentum components. We consider a trajectory to be periodic if the variance $\sigma^2(\tilde{h}_3)$ is less than 0.175. The variance of $\tilde{h}_3$ is much less than the variance in the other two directions since limit cycles are centered about the major axis spin fixed point and are bounded by the unperturbed heteroclinic orbits. We have found that the value 0.175 is the smallest value of $\sigma^2(\tilde{h}_3)$ for which the computer is able to correctly identify each visually identified periodic orbit.

Measure III. If a trajectory failed either of the previous two variance conditions we deemed it to be chaotic. Several visually identified chaotic trajectories are used to verify that the algorithm is able to differentiate between the different trajectory types.

Investigation and Discussion of Results

Analytical Results: The Melnikov Criterion. We begin by qualitatively studying Eq. (44) to see what can be learned about chaos in this system. It can be seen that no immediate conclusions can be drawn about the dependence on the parameters $\tilde{\eta}$, $\tilde{\Omega}$, r_1, and r_2 since Eq. (44) is such a complicated function of each of these parameters. On the other hand, we can immediately see that as the rotor inertia $\tilde{I}_r$ is increased, it becomes more difficult to achieve chaos. In addition, as the damping $\tilde{\gamma}$ is increased, it becomes increasingly *easier* to have chaos. This damping result is counter to what one might expect in a mechanical system—that increased damping *suppresses* chaos, not enhances it.

Further investigation reveals that the $\tilde{I}_r$ and $\tilde{\gamma}$ results are consistent with the dynamics. To see this, we define the *settling time* as the time required for the kinetic energy to decay through 95 percent of the difference between the initial kinetic energy and the minimum kinetic energy state. Figure 7 shows the settling time of the kinetic energy for the damped, *unperturbed* rigid body when γ and I_r (the dimensional quantities) are independently varied.[4] It is immediately clear that as the rotor inertia is increased, kinetic energy is dissipated more quickly. This is consistent with the above observation that as $\tilde{I}_r$ is increased, chaos is more easily achieved and with the idea that increased energy dissipation tends to suppress chaos. It is the relative angular velocity, $\tilde{\omega}_r$, between the carrier body and the rotor that produces the damping. It seems, therefore, that as the rotor inertia $\tilde{I}_r$ is increased it is more difficult to get the rotor spinning and therefore the relative angular velocity between the rotor and the carrier body is increased, leading to an increased energy dissipation rate.

Similarly, as the viscous damping coefficient is initially increased from a small value, the energy dissipation rate increases, as expected. However, as the viscous damping coefficient is increased further, the coupling between the carrier body and the rotor becomes stronger, thus restricting the relative movement between the two bodies and thus $\tilde{\omega}_r$. For large values of $\tilde{\gamma}$, the increased coupling predominates and damping is diminished, and for small values of $\tilde{\gamma}$, damping is decreased because there is little viscosity. It is expected that there should be an optimal value for $\tilde{\gamma}$ such that the rate of damping or kinetic energy dissipation is maximized. This effect is easily seen in Fig. 7 as well as in Fig. 8, which illustrates the system's kinetic energy time histories for various values of damping. Since we have assumed that $\tilde{\gamma} = \mathcal{O}(1)$, our Melnikov result is exhibiting behavior consistent with the right half of the damping curve in Fig. 7—increasing $\tilde{\gamma}$ decreases energy dissipation and therefore makes chaos easier to attain.

Since the parameter space for studying the boundaries between chaotic and nonchaotic motion is six-dimensional, we investigate three-dimensional subspaces by fixing three of the parameters and

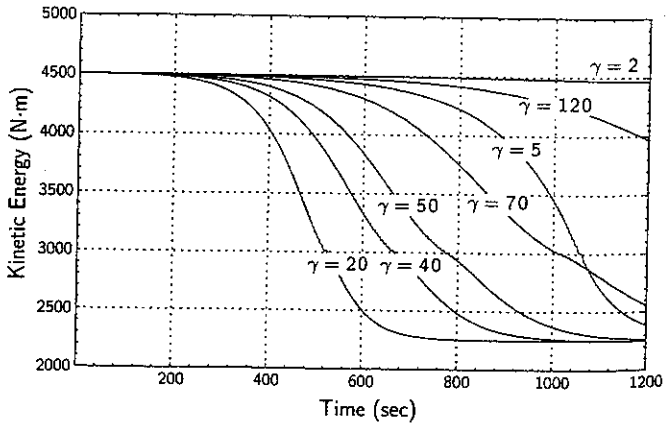

Fig. 8 Rigid-body kinetic energy as a function of time for different values of damping γ

[4] Figures 7 and 8 integrate the unperturbed dimensional equations of motion (Eqs. (1)–(4) with $\Delta = 0$) for $A = 1000$ kg · m^2, $B = 1500$ kg · m^2, and $C = 2000$ kg · m^2.

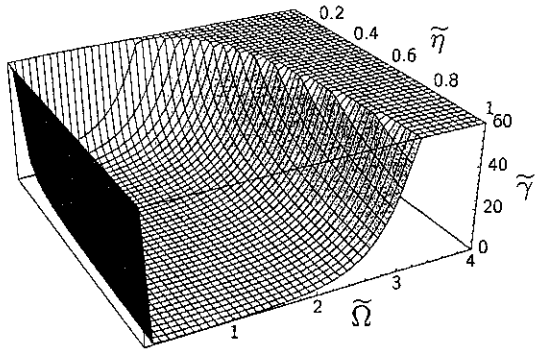

Fig. 9 Surface separating chaotic from nonchaotic motion in $\tilde{\gamma}$, $\tilde{\eta}$, $\tilde{\Omega}$ space. $r_1 = 1.5$, $r_2 = 0.6$, and $\tilde{I}_r = 1.0$.

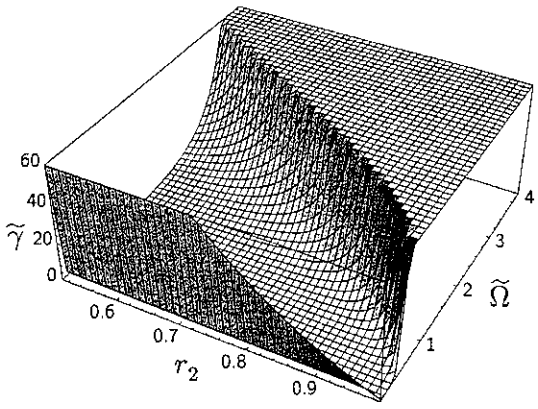

Fig. 12 Surface separating chaotic from nonchaotic motion in $\tilde{\gamma}$, r_2, $\tilde{\Omega}$ space. $\tilde{\eta} = 0.75$, $r_1 = 1.5$, and $\tilde{I}_r = 1.0$.

then plotting the other three. The surface shown in Fig. 9 shows the boundary between chaotic and nonchaotic motion in $\tilde{\gamma}$, $\tilde{\eta}$, $\tilde{\Omega}$ space. In this figure, and all figures that follow, points in parameter space *above* the surface are chaotic. We also note that the drastic change in slope that occurs for small values of $\tilde{\Omega}$ in Figs. 9, 11, and 12 is a result of practical limits on plotting resolution. In reality, the surface does rise sharply for small $\tilde{\Omega}$, but does so smoothly (see detailed cross section in Fig. 10). In any case, we note that the Melnikov result is not valid for very small $\tilde{\Omega}$, since we have assumed that $\tilde{\Omega} = \mathcal{O}(1)$. Figure 9 shows, as expected, that for $\tilde{\eta} = 0$, chaotic motion is impossible for all values of $\tilde{\Omega}$ and $\tilde{\gamma}$—without a time-dependent perturbation, chaos cannot occur. We also see the inverse dependence of the chaos criterion on $\tilde{\gamma}$—chaos occurs for larger values of $\tilde{\gamma}$ instead of smaller.

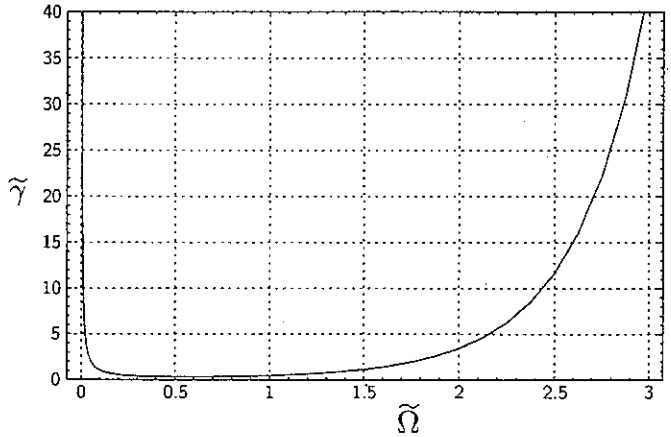

Fig. 10 Cross section of Fig. 9. Line separating chaotic from nonchaotic motion in $\tilde{\gamma}$, $\tilde{\Omega}$ space. $r_1 = 1.5$, $r_2 = 0.6$, $\tilde{I}_r = 1.0$, and $\tilde{\eta} = 0.9$.

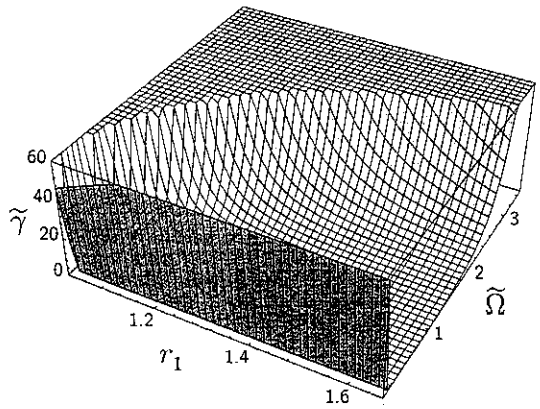

Fig. 11 Surface separating chaotic from nonchaotic motion in $\tilde{\gamma}$, r_1, $\tilde{\Omega}$ space. $\tilde{\eta} = 0.75$, $r_2 = 0.667$, and $\tilde{I}_r = 1.0$.

Figure 11 shows the dependence of the criterion for chaos on the shape of the rigid body. We see that for values of $r_1 \to 1$, which corresponds to a nearly symmetric prolate body, no chaotic motion occurs. Analogous to the previous figure, as the forcing frequency $\tilde{\Omega} \to 0$, no chaotic motion occurs since a zero forcing frequency implies no perturbation. As in Fig. 11, Fig. 12 shows the chaotic dependence on the shape of the rigid body, but this time for r_2 instead of r_1. We see that for $r_2 \to 1$, chaotic motion is impossible to obtain for any value of $\tilde{\gamma}$ or $\tilde{\Omega}$. This shape corresponds to a nearly symmetric oblate carrier body. Figures 13 and 14 show many of the same trends that the previous three figures did, but they also show the chaotic dependence on $\tilde{\eta}$. As $\tilde{\eta} \to 0$ there can be no chaotic motion since that implies a zero perturbation. In addition, we see that as we increase $\tilde{\eta}$, chaotic motion is assured for all values of the system parameters—a large enough perturbation can overcome all other factors.

Comparison Numerical and Melnikov Results. The summary of numerical simulations shown in Fig. 3 demonstrate that

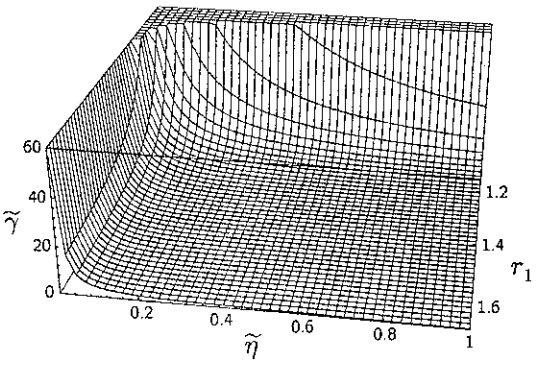

Fig. 13 Surface separating chaotic from nonchaotic motion in $\tilde{\gamma}$, r_1, $\tilde{\eta}$ space. $\tilde{\Omega} = 1.0$, $r_2 = 0.667$, and $\tilde{I}_r = 1.0$.

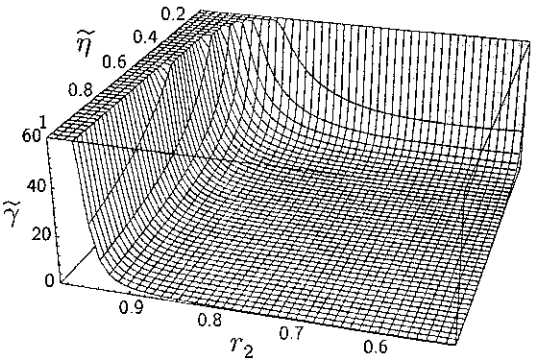

Fig. 14 Surface separating chaotic from nonchaotic motion in $\tilde{\gamma}$, r_2, $\tilde{\eta}$ space. $\tilde{\Omega} = 1.0$, $r_1 = 1.5$, and $\tilde{I}_r = 1.0$.

Melnikov's method, though very conservative in some regions of parameter space, clearly gives a good bound in others. In addition, within the accuracy of the parameter mesh chosen, there appear to be no "nonlinear" points in parameter space (those that lead to chaotic or limit cycle trajectories) that are not captured by the Melnikov curve. Extensive additional numerical simulation for many other ranges of the parameter values does not contradict these results.

Conclusion

We have derived an analytical criterion for the occurrence of a chaotic region of phase space in terms of system parameters for a viscously damped rigid body with time-periodic perturbations. The analytical criterion for the occurrence of chaos is obtained by applying Melnikov's method to a perturbed, viscously damped rigid-body model. It is obvious from the modern theory of nonlinear dynamics that chaos can occur via the breakup of heteroclinic orbits in this class of systems. The contribution of this paper is the formulation of physically reasonable spacecraft models, using rigid-body approximations, to which Melnikov's method can be applied and the performance of the difficult calculations required to obtain an uncomplicated criterion for chaos that can easily be used for spacecraft design. We have also explained a result that was, at first, "counterintuitive" to us—increased viscous damping *enhances* the onset of chaotic dynamics. This is an important consideration when placing viscous dampers on spacecraft.

In addition, subspaces of the full-parameter space are studied analytically and numerically to obtain a qualitative and quantitative understanding of the interactions of the various parameters leading to nonlinear motion. The complete Melnikov result is easily used to obtain the quantitative information needed when a spacecraft and its subsystems are being designed. Numerical simulations indicate that the Melnikov result, though conservative, gives investigators an excellent gauge on the region of parameter space in which to look for nonlinear motion. Future work will extend this approach to better understand the onset of chaos in other classes of spacecraft and to attempt to obtain a fundamental understanding of the important factors leading to unpredictable chaotic dynamics.

Acknowledgments

We would like to thank the reviewers of this paper for pointing out some technical issues, which, though they did not change the results, led us to a much deeper understanding of our work. The third author gratefully acknowledges funding in part by NSF PYI grant ECS-9157192.

References

Adams, G. J., 1980, "Dual-Spin Spacecraft Dynamics During Platform Spinup," *Journal of Guidance and Control,* Vol. 3, No. 1, pp. 29–36.

Baillieul, J., and Levi, M., 1987, "Rotational Elastic Dynamics," *Physica,* Vol. 27D, pp. 43–62.

Barba, P. M., Furumoto, N., and Leliakov, I. P., 1973, "Techniques for Flat-Spin Recovery of Spinning Satellites," *AIAA Guidance and Control Conference,* Key Biscayne, Florida, AIAA paper 73-859.

Barba, P. M., and Aubrun, J. N., 1976, "Satellite Attitude Acquisition by Momentum Transfer," *AIAA Journal,* Vol. 14, No. 10, pp. 1382–1386.

Campbell, D. R., III, 1997, "Analytical and Numerical Analysis of Nonlinear Phenomena for a Class of Spacecraft Attitude Acquisition Maneuvers," Ph.D. dissertation, The Pennsylvania State University, University Park, PA.

Chinnery, A. E., and Hall, C. D., 1995, "Motion of a Rigid Body with an Attached Spring-Mass Damper," *Journal of Guidance, Control, and Dynamics,* Vol. 18, No. 6, pp. 1404–1409.

Cochran, J. E., and Holloway, H. E., 1980, "Resonances in the Attitude Motions of Asymmetric Dual-Spin Spacecraft," *The Journal of the Astronautical Sciences,* Vol. 28, No. 3, pp. 231–254.

Cronin, D. L., 1978, "Flat Spin Recovery of a Rigid Asymmetric Spacecraft," *Journal of Guidance and Control,* Vol. 1, No. 4, pp. 281–282.

Dovbysh, S. A., 1989, "Some New Dynamical Effects in the Perturbed Euler-Poinsot Problem Due to Splitting of Separatrices," *Journal of Applied Mathematics and Mechanics,* Vol. 53, No. 2, pp. 165–173.

Gebman, J. R., and Mingori, D. L., 1976, "Perturbation Solution for the Flat Spin Recovery of a Dual-Spin Spacecraft," *AIAA Journal,* Vol. 14, No. 7, pp. 859–867.

Gray, G. L., Dobson, I., and Kammer, D. C., 1996, "Chaos in a Spacecraft Attitude Maneuver Due to Time-Periodic Perturbations," ASME JOURNAL OF APPLIED MECHANICS, Vol. 63, pp. 501–508.

Gray, G. L., Kammer, D. C., and Dobson, I., 1992, "Chaos in an Attitude Maneuver of a Damped Satellite Due to Time-Periodic Perturbations," *AAS/AIAA Spaceflight Mechanics Conference,* Colorado Springs, CO, Paper AAS 92-171.

Gray, G. L., Mazzoleni, A. P., and Campbell, D. R., III, 1998, "Analytical Criterion for Chaotic Dynamics in Flexible Satellites with Nonlinear Controller Damping," *Journal of Guidance, Control, and Dynamics,* Vol. 21, No. 4, pp. 558–565.

Guckenheimer, J., and Holmes, P., 1983, *Nonlinear Oscillations, Dynamical Systems, and Bifurcations of Vector Fields,* Springer-Verlag, New York.

Hall, C. D., and Rand, R. H., 1994, "Spinup Dynamics of Axial Dual-Spin Spacecraft," *Journal of Guidance, Control, and Dynamics,* Vol. 17, No. 1, pp. 30–37.

Hindmarsh, A. C., 1983, "ODEPACK, A Systematized Collection of ODE Solvers," *Scientific Computing,* R. S. Stepleman et al., eds., North-Holland, Amsterdam, pp. 55–64. (Also see http://gams.nist.gov/ to obtain the source code.)

Holmes, P. J., 1980, "Averaging and Chaotic Motions in Forced Oscillations," *SIAM Journal of Applied Mathematics,* Vol. 38, No. 1, pp. 65–80.

Holmes, P. J., 1981, "Errata and Addenda: Averaging and Chaotic Motions in Forced Oscillations," *SIAM Journal of Applied Mathematics,* Vol. 40, No. 1, pp. 167–168.

Holmes, P., 1983, "Bifurcation and Chaos in a Simple Feedback Control System," *Proceedings of the 22nd IEEE Conference on Decision and Control,* San Antonio, TX, IEEE, Piscataway, NJ, pp. 365–370.

Holmes, P. J., and Marsden, J. E., 1983, "Horseshoes and Arnold Diffusion for Hamiltonian Systems on Lie Groups," *Indiana University Mathematics Journal,* Vol. 32, No. 2, pp. 273–309.

Hughes, P. C., 1986, *Spacecraft Attitude Dynamics,* John Wiley and Sons, New York.

Kaplan, M. H., and Cenker, R. J., 1973, "Control of Spin Ambiguity During Reorientation of an Energy Dissipating Body," *Journal of Spacecraft and Rockets,* Vol. 10, No. 12, pp. 757–760.

Koiller, J., 1984, "A Mechanical System with a 'Wild' Horseshoe," *Journal of Mathematical Physics,* Vol. 25, No. 5, pp. 1599–1604.

Krishnaprasad, P. S., 1985, "Lie-Poisson Structures, Dual-Spin Spacecraft and Asymptotic Stability," *Nonlinear Analysis, Theory, Methods & Applications,* Vol. 9, No. 10, pp. 1011–1035.

Krishnaprasad, P. S., and Marsden, J. E., 1987, "Hamiltonian Structures and Stability for Rigid Bodies with Flexible Attachments," *Archive for Rational Mechanics and Analysis,* Vol. 98, No. 1, pp. 71–93.

Levi, M., 1989, "Morse Theory for a Model Space Structure," *Proceedings of the AMS-IMS-SIAM Joint Summer Research Conference in the Mathematical Sciences on Control Theory and Multibody Systems,* Bowdoin College, Brunswick, ME, J. E. Marsden, P. S. Krishnaprasad, and J. C. Simo, eds., in the series *Contemporary Mathematics,* Vol. 97, American Mathematical Society, Providence, RI, pp. 209–216.

Lichtenberg, A. J., and Lieberman, M. A., 1992, *Regular and Chaotic Dynamics,* 2nd Ed., Springer-Verlag, New York.

Longuski, J. M., and Tsiotras, P., 1993a, "Analytic Solution for a Spinning Rigid Body Subject to Time-Varying Body-Fixed Torque, Part I: Constant Axial Torque," ASME JOURNAL OF APPLIED MECHANICS, Vol. 60, No. 4, pp. 970–975.

Longuski, J. M., and Tsiotras, P., 1993b, "Analytic Solution for a Spinning Rigid Body Subject to Time-Varying Body-Fixed Torque, Part II: Time-Varying Body-Fixed Torque," ASME JOURNAL OF APPLIED MECHANICS, Vol. 60, pp. 976–981.

Melnikov, V. K., 1963, "On the Stability of the Center for Time-Periodic Perturbations," *Transactions of the Moscow Mathematical Society,* Vol. 12, pp. 1–56.

Or, A. C., 1991, "Resonances in the Despin Dynamics of Dual-Spin Spacecraft," *Journal of Guidance, Control, and Dynamics,* Vol. 14, No. 2, pp. 321–329.

Or, A. C., 1998a, "Chaotic Motions of a Dual-Spin Body," ASME JOURNAL OF APPLIED MECHANICS, Vol. 65, pp. 150–156.

Or, A. C., 1998b, "Dynamics of an Asymmetric Gyrostat," *Journal of Guidance, Control, and Dynamics,* Vol. 21, No. 3, pp. 416–420.

Rahn, C. D., and Barba, P. M., 1991, "Reorientation Maneuver for Spinning Spacecraft," *Journal of Guidance, Control, and Dynamics,* Vol. 14, No. 4, pp. 724–728.

Rubanovskii, V. N., 1988, "On the Relative Equilibria of a Satellite-Gyrostat, Their Branchings and Stability," *Journal of Applied Mathematics and Mechanics,* Vol. 52, No. 6, pp. 710–714.

Tong, X., and Tabarrok, B., 1997, "Bifurcation of Self-Excited Rigid Bodies Subjected to Small Perturbation Torques," *Journal of Guidance, Control, and Dynamics,* Vol. 20, No. 1, pp. 123–128.

Tsiotras, P., and Longuski, J. M., 1991, "A Complex Analytic Solution for the Attitude Motion of a Near-Symmetric Rigid Body Under Body-Fixed Torques," *Celestial Mechanics and Dynamical Astronomy,* Vol. 51, No. 3, pp. 281–301.

Volosov, V. M., 1962, "Averaging in Systems of Ordinary Differential Equations," *Russian Mathematical Surveys,* Vol. 17, pp. 1–126.

Wiggins, S., 1990, *Introduction to Applied Nonlinear Dynamical Systems and Chaos,* Springer-Verlag, New York.

Transactions of the ASME®

Technical Editor: LEWIS T. WHEELER
Department of Mechanical Engineering
University of Houston
Houston, TX 77204-4792

Transactions of the ASME, Journal of Applied Mechanics (ISSN 0021-8936) is published quarterly (Mar., June, Sept., Dec.) for $250.00 per year by The American Society of Mechanical Engineers, Three Park Avenue, New York, NY 10016.

Periodicals postage paid at New York, NY and additional mailing office. POSTMASTER: Send address changes to Transactions of the ASME, Journal of Applied Mechanics c/o THE AMERICAN SOCIETY OF MECHANICAL ENGINEERS, 22 Law Drive, Box 2300, Fairfield, NJ 07007-2300.

CHANGES OF ADDRESS must be received at Society headquarters seven weeks before they are to be effective. Please send old label and new address. PRICES: To members, $40.00; to nonmembers, $250.00; single issue, $100.00. Add $40.00 (airmail $60.00) for postage to countries outside the United States and Canada.

Journal of Applied Mechanics

Published Quarterly by The American Society of Mechanical Engineers

VOLUME 66 • NUMBER 3 • SEPTEMBER 1999

TECHNICAL PAPERS

(Contents continued on outside back cover)

This journal is printed on acid-free paper, which exceeds the ANSI Z39.48-1992 specification for permanence of paper and library materials. ⊗™
♻ 85% recycled content, including 10% post-consumer fibers.